International Journal of Naval Architecture and Ocean Engineering 10 (2018) 683–691

Contents lists available at ScienceDirect

International Journal of Naval Architecture and Ocean Engineering

journal homepage: http://www.journals.elsevier.com/international-journal-of-naval-architecture-and-ocean-engineering/

The sensitivity of ship resistance to wall-adjacent grids and near-wall treatments

Dong Woo Park [a], Sang Bong Lee [b, *]

[a] Department of Naval Architecture and Ocean Engineering, TongMyong University, Busan, South Korea
[b] Department of Naval Architecture and Offshore Engineering, Dong-A University, Busan, South Korea

ARTICLE INFO

Article history:
Received 7 August 2017
Received in revised form
18 October 2017
Accepted 17 December 2017
Available online 12 January 2018

ABSTRACT

Numerical simulations of turbulent flows around KCS have been performed to study the sensitivity of ship resistance to wall-adjacent grids and disclose the influence of near-wall treatment on the sensitivity of ship resistance. The resistance coefficients of viscous and pressure forces were compared when using realizable k-ε and SST k-ω turbulence models in structured and unstructured grids, respectively. The calculation of friction velocity was found to be mainly responsible for the reduction of viscous and total resistances when the height of wall-adjacent cells increased. Since the assumption of equilibrium state between turbulent production and dissipation was not met in a bulbous bow, it was more reasonable to iteratively calculate the friction velocity from empirical laws of the wall for near-wall treatment rather than explicitly estimate it from the turbulent kinetic energy.

1. Introduction

The calculation of ship resistance with high precision is essential to making the best choice among several hull forms where the resistance performance is of major concern. High precision of numerical solutions has mostly been achieved by generating the same surface and volume meshes around hulls in structured grid systems for which users could directly control grid sizes. Grid verification is a typical process of examining the precision of numerical solutions by quantifying grid uncertainty while the grid size increases or decreases at a constant rate (Wilson et al., 2001; Banks et al., 2010; Guo et al., 2013). Once a grid system around hulls has been well verified, the grid uncertainty of grid system can be quantitatively evaluated based on the rate of grid manipulation and the order of spatial discretization schemes. This means that the verified grid system can be used to make a reliable comparison of ship resistance among several hull forms. The high precision of ship resistance in the verified grid system, however, is not able to guarantee that an increase of grid numbers automatically will lead to agreement of numerically predicted ship resistance with experimental value, i.e., high accuracy of numerical solution. If the purpose of numerical simulation is to know which hull is best for resistance performance, a numerical process with high precision and low accuracy can be available to predict the force acting on a hull. But ship resistance has to be numerically predicted with high accuracy if self-propulsion performance is of major concern for the comparison of hull forms. This is because both thrust acting on a propeller and resistance acting on a hull play important roles in the prediction of self-propulsion performance (Choi et al., 2010). This is one of the reasons why numerical evaluation of self-propulsion performance is more difficult than that of resistance performance.

Recently, Lee (2014) has performed a wide scope of numerical simulations to accurately predict ship resistance. The numerical results of 264 cases have been compared with experimental measurements of towing tank tests in order to analyze the statistical reliability of numerical procedures. In his study the numerical error was estimated to be as small as ±2% with a 95% confidence level when Reynolds averaged Navier-Stokes equations with a wall function were solved by using STAR-CCM+ and OpenFOAM, respectively. In order to achieve high accuracy of numerical solutions the height of wall-adjacent cells was adjusted by employing a nonlinear function of viscosity, velocity and ship length because he found ship resistance to be sensitive to grid system and near-wall treatment of wall function. Based on his numerical method, Kim and Park (2017) developed HiFoam to efficiently predict the ship resistance. However the previous studies did not systematically report the influence of the grid system and near-wall treatment on

* Corresponding author.
E-mail address: sblee1977@dau.ac.kr (S.B. Lee).
Peer review under responsibility of Society of Naval Architects of Korea.

https://doi.org/10.1016/j.ijnaoe.2017.12.003

Nomenclature

C_{PM}	resistance coefficient of pressure force
C_{TM}	total resistance coefficient
C_{VM}	resistance coefficient of viscous force
g	gravity acceleration
G_k	production term of turbulent kinetic energy
k	turbulent kinetic energy
L_{pp}	length between perpendiculars
p	pressure
t	time
U	velocity of mixture
U_Γ	velocity for artificial compression
u_τ	friction velocity
V_M	velocity of model ship
x, y, z	coordinate system
α	volume fraction
ε	turbulent dissipation rate
η	normal distance from cell centroid to wall
η^*	dimensionless normal distance from cell centroid to wall
$\Delta\eta_{wall}$	height of wall-adjacent cells
κ	von Karman constant
μ	dynamic viscosity
ρ	density
ν	kinematic viscosity
τ_w	wall shear stress
ω	specific dissipation rate
air	air
water	water

ship resistance although the wall shear stress of OpenFOAM was found to be very sensitive to the height of cells adjacent to the wall as well as the boundary condition of turbulent viscosity at the wall. The sensitivity of OpenFOAM might be caused by the calculation of wall shear stress from an effective viscosity multiplied by the velocity gradient at the wall.

The main objectives of the present study are to investigate the sensitivity of ship resistance to wall-adjacent grids and disclose the influence of near-wall treatment on the sensitivity of ship resistance in the framework of OpenFOAM. To do this the resistance coefficients of viscous and pressure forces acting on the hull are compared when using realizable k-ε and SST k-ω turbulence models in structured and unstructured grids, respectively. The formulation of turbulent kinetic energy production and the numerical procedure for calculating the friction velocity on the hull will be discussed for near-wall treatment in detail. In the present study we utilize OpenFOAM to numerically predict the resistances of KRISO container ship (KCS).

2. Numerical methods

Because details of the numerical method and the formulation of governing equations for incompressible turbulent multiphase flows have been extensively documented in many literature, we briefly describe the main features of the numerical methods used in the present work.

2.1. Governing equations

The mass and momentum conservation equations to obtain velocity and pressure for incompressible turbulent two-phase flow around a hull are expressed as follows:

$$\frac{\partial \alpha}{\partial t} + \nabla\cdot(\alpha\vec{U}) + \nabla\cdot[\alpha(1-\alpha)\vec{U}_\Gamma] = 0 \tag{1}$$

$$\frac{\partial}{\partial t}(\rho\vec{U}) + \nabla\cdot(\rho\vec{U}\vec{U}) = -\nabla p + \nabla\cdot\left[(\mu+\mu_t)\left\{\nabla\vec{U} + \nabla\vec{U}^T - \frac{2}{3}\nabla\cdot\vec{U}I\right\}\right] + \rho\vec{g} \tag{2}$$

where $\vec{U}$ is a velocity vector of mixtures and $\vec{U}_\Gamma$ is a velocity field for an extra artificial compression term that serves to capture the sharp interface between water and air (Rusche, 2002). Because the present two-phase flow is concerned with the Volume of Fluid (VOF) method, the scalar function of volume fraction for water is $\alpha(x,t)\in[0,1]$. The density and dynamic viscosity of mixtures are expressed, respectively, as follows:

$$\rho = \alpha\rho_{water} + (1-\alpha)\rho_{air} \tag{3}$$

$$\mu = \alpha\mu_{water} + (1-\alpha)\mu_{air}. \tag{4}$$

The turbulent dynamic viscosity denoted by μ_t in Eq. (2) is calculated from transported variables in two-equation turbulence models. The concept of turbulent viscosity is based on the Boussinesq hypothesis of relating Reynolds stresses to the gradient of mean velocity. In realizable k-ε model the turbulent viscosity is computed by combining the turbulent kinetic energy (k) and turbulent dissipation rate (ε) as follows:

$$\mu_t = \rho C_\mu \frac{k^2}{\varepsilon} \tag{5}$$

where C_μ is a model constant determined from experiments for fundamental turbulent flows such as isotropic turbulence and turbulent boundary layers. The turbulent kinetic energy and dissipation rate are obtained from the following transport equations:

$$\frac{\partial}{\partial t}(\rho k) + \nabla\cdot(\rho k\vec{U}) = \nabla\cdot\left[\left(\mu + \frac{\mu_t}{\sigma_k}\right)\nabla k\right] + G_k - \rho\varepsilon \tag{6}$$

$$\frac{\partial}{\partial t}(\rho\varepsilon) + \nabla\cdot(\rho\varepsilon\vec{U}) = \nabla\cdot\left[\left(\mu + \frac{\mu_t}{\sigma_\varepsilon}\right)\nabla\varepsilon\right] + C_{1\varepsilon}\frac{\varepsilon}{k}G_k - C_{2\varepsilon}\rho\frac{\varepsilon^2}{k} \tag{7}$$

where σ_k, σ_ε, $C_{1\varepsilon}$, $C_{2\varepsilon}$ are model constants and G_k represents a production term of turbulent kinetic energy from the gradient of mean velocity, i.e., $G_k = \mu_t S^2$. The modulus of strain rate tensor of mean velocity is defined by $S\equiv\sqrt{S_{ij}S_{ij}}$ where $S_{ij} = \frac{1}{2}\left(\frac{\partial U_j}{\partial x_i} + \frac{\partial U_i}{\partial x_j}\right)$.

Shear stress transport (SST) k-ω model of Menter et al. (2003) computes the turbulent viscosity by combining k and the specific dissipation rate (ω) as follows:

$$\mu_t = \frac{\rho a_1 k}{\max[a_1\omega, SF_2]} \tag{8}$$

where F_2 is a blending function. The turbulent kinetic energy and the specific dissipation rate are computed from the following

transport equations:

$$\frac{\partial}{\partial t}(\rho k) + \nabla\cdot\left(\rho k\overrightarrow{U}\right) = \nabla\cdot[(\mu + \sigma_k\mu_t)\nabla k] + G_k - \beta^*\rho\omega k \tag{9}$$

$$\frac{\partial}{\partial t}(\rho\omega) + \nabla\cdot\left(\rho\omega\overrightarrow{U}\right) = \nabla\cdot[(\mu + \sigma_\omega\mu_t)\nabla\omega] + \frac{\rho\gamma}{\mu_t}G_k - \beta\rho\omega^2 + 2(1-F_1)\frac{\rho\sigma_{\omega 2}}{\omega}\nabla k\nabla\omega \tag{10}$$

where σ_k, β^*, σ_ω, γ, β, $\sigma_{\omega 2}$ are model constants and F_1 is a blending function.

2.2. Grid systems

Table 1 describes the principal particulars of the object ship used in the present study, 3600 TEU container carrier KCS (Kim et al., 2001). We performed numerical simulations under the fixed condition of a model ship. Fig. 1 illustrates the structured and unstructured grids for multiphase simulations with VOF model, from which the ship resistance is obtained. The structured grids of O–H type are generated with reference to the hexahedral grid systems of which uncertainty analysis has been performed in a previous study (Choi et al., 2010). The structured grids are carefully generated to keep the orthogonality of cells adjacent to the free surface as seen in Fig. 1(a). The inlet and outlet boundaries of structured grids are located $1.0L_{PP}$ upstream and $1.5L_{PP}$ downstream from the mid-ship, respectively. The distance between the far-field boundary and the hull is $1.0L_{PP}$, where L_{PP} represents the length between perpendiculars. To investigate the sensitivity of ship resistance to the height of wall-adjacent cells ($\Delta\eta_{wall}$), $\Delta\eta_{wall}$ is only adjusted from 0.0015 m to 0.012 m on the same structured grid where the total number of hexahedral cells is kept constant (1,532,968). The inlet velocity is set to be a constant 2.1762 m/s, while Neumann boundary condition is used at the outlet boundary. Physical properties are assumed to be symmetric at the far-field, top and symmetry boundaries. The positive x- and y-axes are in the streamwise and starboard directions respectively. The positive z-axis is the upward direction.

The present unstructured grids are generated using adapted meshes with prism layers near the hull, which method has been used by Lee (2014) in a previous study. The domain of unstructured grids is a rectangular shape with the inlet and outlet boundaries being located $1.5L_{PP}$ upstream and $2.5L_{PP}$ downstream from the mid-ship, respectively. Although we unequally use the present domain sizes of structured and unstructured grids, we found in preliminary simulations that the ship resistance was little affected by an extension of the numerical domains unless the domain size was smaller than that of the structured grids. Note that we place the main focus of the present study not on a comparison of ship resistances between structured and unstructured grids, but on the sensitivity of ship resistance to wall-adjacent cells of structured and unstructured grids. $\Delta\eta_{wall}$ of the present unstructured grids changes from 0.0015 m to 0.012 m by controlling the thickness of the first prism layer attached to the hull. Table 2 shows that unlike in structured grids the total number of cells is not constant in unstructured grids because the surface and volume cells are automatically generated. When the stretching ratio and total thickness of prism layers changes, we also describe the total number of cells in the table. The inlet, outlet, top and symmetry boundary conditions are the same as those of the structured grids. In addition the symmetric boundary condition is given at the bottom and side boundaries of unstructured grids.

Table 1
Principal particulars of KCS.

	Full scale	Model scale
length (L_{PP})	230.0m	7.2786m
breadth	32.2m	1.0190m
depth	19.0m	0.6013m
draft	10.8m	0.3418m
wetted surface area	9498.0m^2	9.5121m^2
scale ratio	1	1/31.6
speed	24knots	2.1964 m/s

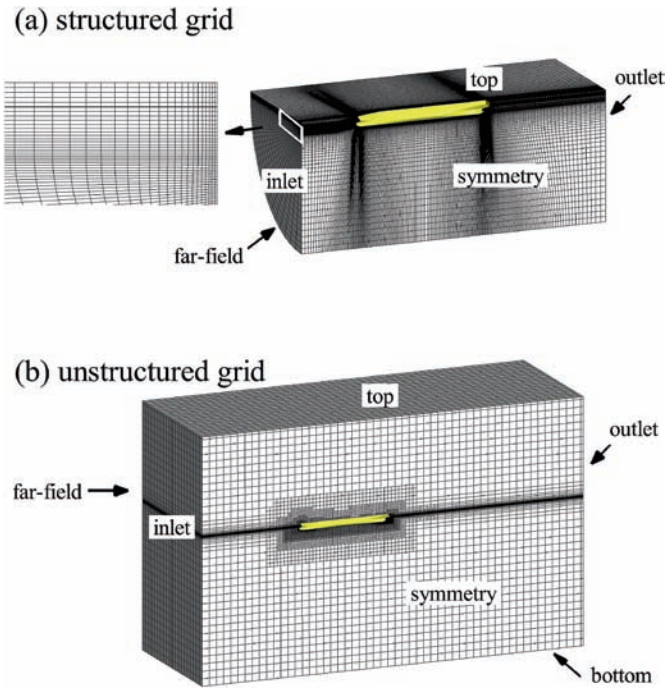

Fig. 1. Numerical domains of structured and unstructured grids.

2.3. Numerical schemes

A very efficient Local time Stepping (LTS) scheme is implemented for temporal discretization where the time step is locally manipulated for an individual cell based on a constant Courant number. Even if it can give rise to instantaneous violation against physical conservation for mass and momentum, LTS scheme makes it as soon as possible to enable the simulation to reach the steady-state conservation for mass and momentum. The scheme has been efficiently used in multiphase flows where the final solution of numerical simulation was steady (Cowles, 2001). In order to check the physical conservation of mass and momentum in the present study we change the temporal discretization scheme from LTS scheme to Euler scheme after the resistance has converged. A linear interpolation with van Leer limiter is used as a flux limiter of Total Variation Diminishing (TVD) for velocity, k, ε and ω (van Leer, 1979). High Resolution Interface Capturing (HRIC) scheme is implemented to discretize the convective term of scalar transport equation for the volume fraction. The ship resistances reported in the present results are averaged during 1000 time steps after the solution has statistically converged.

3. Results and discussions

We study sensitivity of resistance coefficients to the height of

Table 2
Number of cells in unstructured grids.

$\Delta\eta_{wall}$(m)	Stretching ratio of prism layers	No. layers	Thickness of layers (m)	No. hull faces	No. cells
0.0015	1.3	6	0.01913	30,067	919,927
0.0030	1.1	9	0.04074	29,312	968,170
	1.3	3	0.01197	30,196	833,367
		6	0.03827	29,499	886,725
		10	0.12786	31,612	1,008,451
	1.5	5	0.03956	29,441	856,299
0.0060	1.3	6	0.07654	29,520	873,923
0.0120	1.3	6	0.15307	31,961	881,227

wall-adjacent cells in structured and unstructured grids when using realizable k-ε and SST k-ω turbulence models. The ship resistance for each of cases is listed in Table 3. C_{VM} and C_{PM} represent viscous and pressure contributions to the total resistance coefficient (C_{TM}) acting on the hull, which we express as follows:

$$C_{VM} = \frac{1}{\frac{1}{2}\rho V_M^2 S}\int_S \tau_{wall(x)} dA \tag{11}$$

$$C_{PM} = \frac{1}{\frac{1}{2}\rho V_M^2 S}\int_S p\vec{n}_x \cdot d\vec{A} \tag{12}$$

$$C_{TM} = C_{VM} + C_{PM} \tag{13}$$

where S is a surface area of hull and $\tau_{wall(x)}$ denotes the x component of wall shear stresses acing on a finite hull area of dA. The used heights of wall-adjacent cells in structured grids are 0.0015 m, 0.003 m, 0.006 m and 0.012 m as described in Table 2. The corresponding $\Delta\eta^+$ to each height was also calculated by using friction velocities of SST k-ω model for comparison. We assume the temperature of water to be 15 °C.

A remarkable tendency of resistance coefficients is the decrease of viscous resistance coefficients (C_{VM}) as $\Delta\eta_{wall}$ increases. While the viscous resistance coefficient shows small changes in realizable k-ε model, a relatively large reduction of C_{VM} is observed in SST k-ω model. We observe the largest reduction of C_{VM} in SST k-ω model of unstructured grid while C_{VM} is robust against a change of $\Delta\eta_{wall}$ in a combination of realizable k-ε model and structured grids. From the viewpoint of numerical precision realizable k-ε model with a convergent tendency seems to be more desirable but SST k-ω model is more attractive to improve the numerical accuracy, i.e., it is easier to make a numerical solution of SST k-ω model approximate an experimental value by controlling the height of wall-adjacent cells. The improvement of numerical accuracy by controlling $\Delta\eta_{wall}$ is valid only if the total resistance coefficient (C_{TM}) as well as C_{VM} and C_{PM} are predictable as the height of wall-adjacent cells increases. Unfortunately C_{PM} and C_{TM} of structured grids are likely to be unpredictable in either realizable k-ε model or SST k-ω model. Unlike structured grids, C_{VM} and C_{TM} of SST k-ω model in unstructured grids are approximately proportional to the log-scaled height of wall-adjacent cells regardless of turbulence models while C_{PM} shows little change as shown in Fig. 2. This is an important reason for why Lee (2014) chose an unstructured grid system in the prediction of ship resistance in order to reduce the numerical error to be as small as ±2% with a 95% confidence level. Prior to analyzing the change of resistance coefficients depending on the height of wall-adjacent cells, the sensitivity of resistance coefficients to Gauss linear and least-squares gradient schemes is evaluated in Table 4 and Fig. 3, respectively. As checked, the coefficients are little affected by the gradient schemes because both gradient schemes provide very similar values of velocity gradients in hexahedral cells and most of cells adjacent to the wall are hexahedral in the present study. Hereinafter SST k-ω model shall be used with Gauss linear gradient scheme in the unstructured grids.

The x component of wall shear stresses on the hull is displayed in Fig. 4 when $\Delta\eta_{wall}$ is 0.003 m and 0.012 m in SST k-ω model, respectively. Each coordinate is non-dimensionalized by L_{PP}. As the height of wall-adjacent cells increases low shear stress appears in a bulbous bow of Fig. 4. In order to clarify the local change of wall shear stress resulting from the increase of $\Delta\eta_{wall}$, the difference of $\tau_{wall(x)}$ between $\Delta\eta_{wall} = 0.003$ m and 0.012 m is shown in Fig. 4(d). The decrease of wall shear stress on the bulbous bow is mainly responsible for the reduction of C_{VM} as $\Delta\eta_{wall}$ grows. Despite the predictable approximation of C_{VM} and C_{TM} of SST k-ω model in unstructured grids, it is hard to find a convergence of resistance coefficients with the wall-adjacent grid height. It is because the height of cells adjacent to the wall is only controlled in the present study whereas the Grid Convergence Index (GCI) requires a gradual increase or decrease of all cells in the numerical domain.

The wall shear stress of turbulence models is described as follows:

Table 3
Sensitivity of resistance coefficients to the height of wall-adjacent cells in structured and unstructured grids.

Mesh	$\Delta\eta_{wall}$ (m)	$\Delta\eta^+_{(avg)}$	Realizable k-ε model			SST k-ω model		
			C_{VM}	C_{PM}	C_{TM}	C_{VM}	C_{PM}	C_{TM}
structured	0.0015	44	2.967	0.696	3.662	3.042	0.608	3.651
	0.0030	75	2.967	0.641	3.607	2.973	0.608	3.581
	0.0060	129	2.948	0.576	3.523	2.934	0.642	3.576
	0.0120	219	2.866	0.653	3.520	2.859	0.718	3.578
unstructured	0.0015	38	2.799	0.901	3.700	2.823	0.899	3.722
	0.0030	73	2.787	0.898	3.685	2.721	0.894	3.615
	0.0060	118	2.765	0.889	3.654	2.602	0.914	3.516
	0.0120	191	2.740	0.950	3.690	2.522	0.908	3.430

*The values of C_{VM}, C_{PM} and C_{TM} are scaled by 10^3.
**The experimental value of C_{TM} is 0.003557 under the fixed condition.
***The wall unit of $\Delta\eta$ is calculated by using friction velocities of SST k-ω model.

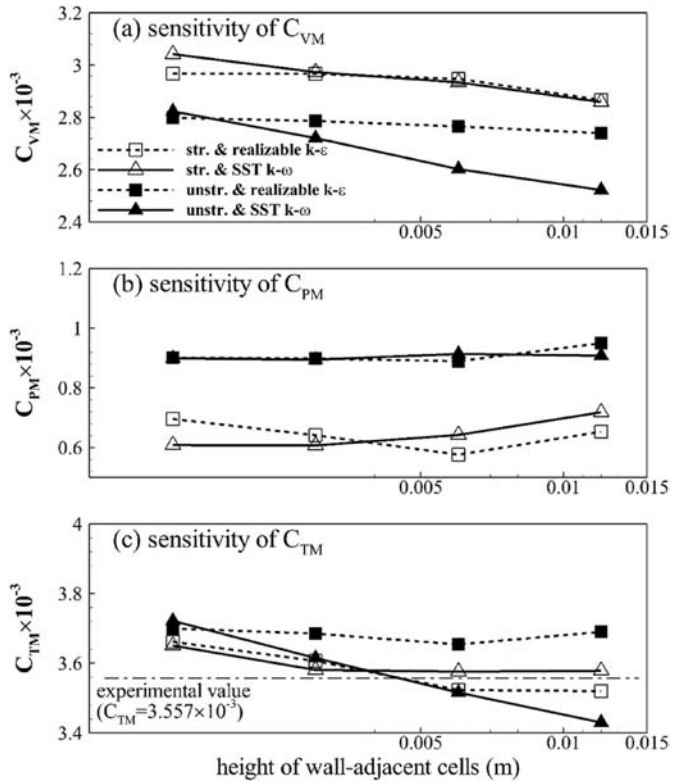

Fig. 2. Sensitivity of resistance coefficients to the height of wall-adjacent cells, where structured and unstructured grids are denoted by 'str.' and 'unstr.' respectively. Experimental value of C_{TM} is displayed by a dash-dot line for reference.

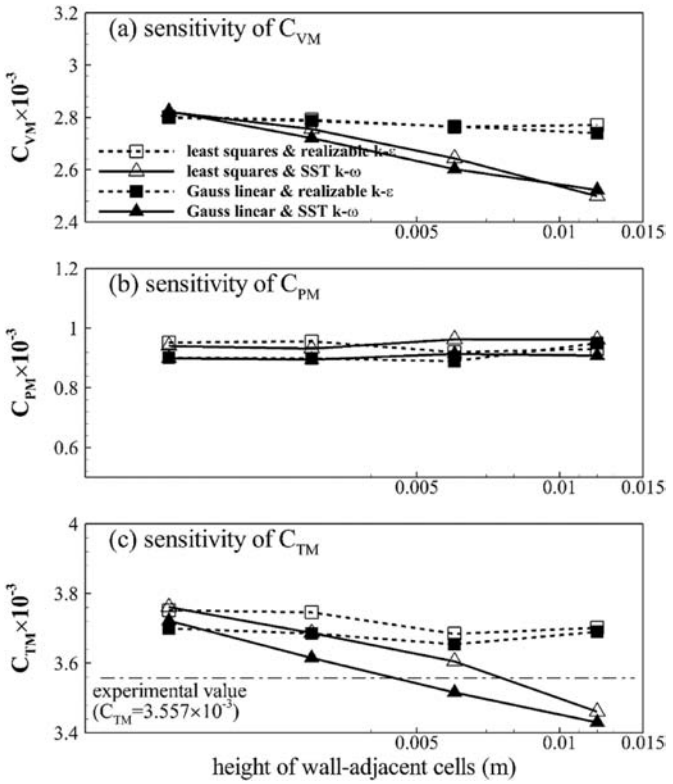

Fig. 3. Sensitivity of resistance coefficients to the gradient scheme in unstructured grids.

$$\tau_w = (\mu_t + \mu)\frac{\partial U}{\partial \eta}\bigg|_{wall} \tag{14}$$

where μ_t and μ represent turbulent and transport dynamic viscosities respectively. The wall shear stress of the log-law is calculated from

$$\tau_w = \frac{\rho U C_\mu^{1/4} k^{1/2}}{U^*} \tag{15}$$

where C_μ is an empirical constant of 0.09 to describe the turbulent viscosity in two-equation turbulence models of RANS (Launder and Spalding, 1972; Craft et al., 2002). Because a dimensionless velocity (U^*) is expressed as $U^* = \kappa^{-1}\log(E\eta^*)$ by the log-law with $E = 9.8$, the wall boundary condition of turbulent kinematic viscosity is given by

$$\nu_t = \nu\left(\frac{\kappa\eta^*}{\log(E\eta^*)} - 1\right) \tag{16}$$

where η^* represents the dimensionless distance from the centroid of wall-adjacent cells to the wall and κ is the von Kármán constant of 0.436. Note that the wall boundary values of turbulent kinematic viscosity are finally determined from the turbulent kinetic energy at wall-adjacent cells. Fig. 5, which displays the turbulent kinetic energy and the turbulent kinematic viscosity at wall-adjacent cells, makes it clear that the low values of turbulent kinetic energy in the bulbous bow cause the reduction of wall shear stress as $\Delta\eta_{wall}$ increases. Since the turbulent kinetic energy is affected by the production of k, the formulation of the turbulent production term (G_k) needs to be checked.

As discussed in the previous study of Park et al. (2013), two formulations of turbulent production term are available for near-wall treatment in turbulent kinetic energy equation. One is

Table 4
Sensitivity of resistance coefficients to the gradient scheme in unstructured grids.

Gradient scheme	$\Delta\eta_{wall}$ (m)	$\Delta\eta^{+}_{(avg)}$	Realizable k-ε model			SST k-ω model		
			C_{VM}	C_{PM}	C_{TM}	C_{VM}	C_{PM}	C_{TM}
Gauss linear	0.0015	38	2.799	0.901	3.700	2.823	0.899	3.722
	0.0030	73	2.787	0.898	3.685	2.721	0.894	3.615
	0.0060	118	2.765	0.889	3.654	2.602	0.914	3.516
	0.0120	191	2.740	0.950	3.690	2.522	0.908	3.430
least squares	0.0015	38	2.801	0.952	3.752	2.821	0.940	3.761
	0.0030	73	2.791	0.956	3.746	2.755	0.931	3.687
	0.0060	115	2.764	0.920	3.684	2.643	0.962	3.605
	0.0120	191	2.771	0.930	3.702	2.499	0.961	3.461

*The values of C_{VM}, C_{PM} and C_{TM} are scaled by 10^3.

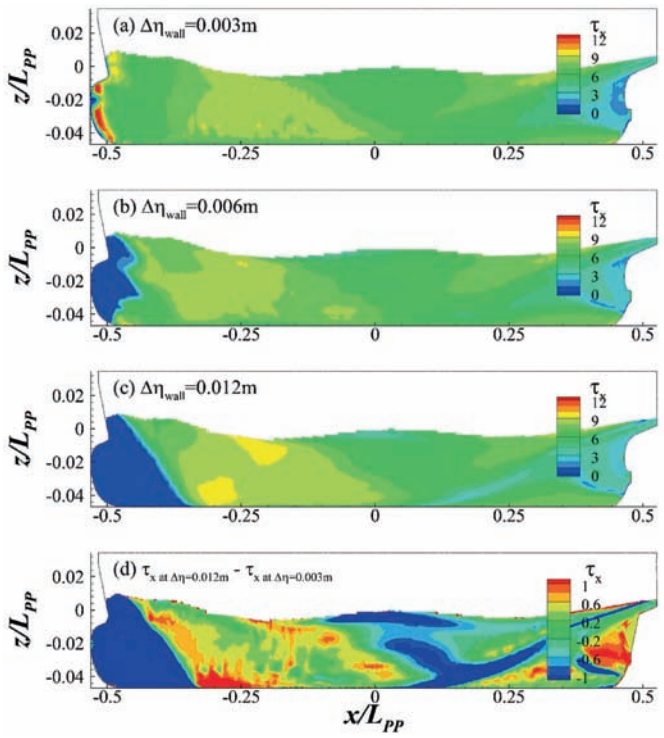

Fig. 4. Sensitivity of wall shear stress on hull to the height of wall-adjacent cells ($\Delta\eta_{wall}$) when $\Delta\eta_{wall}$ increases from 0.003 m to 0.012 m.

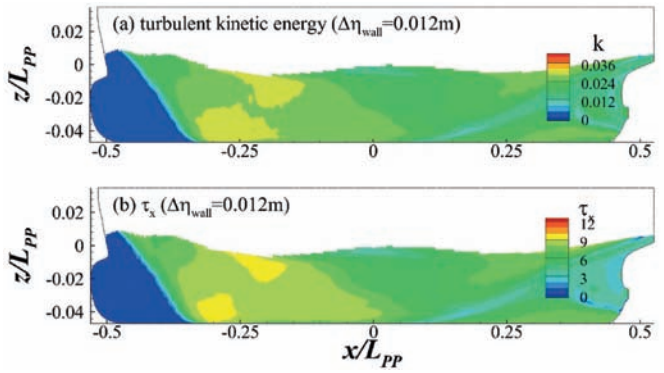

Fig. 5. Comparison of turbulent kinetic energy and x component of wall shear stress when $\Delta\eta_{wall} = 0.012$ m.

expressed as follows

$$G_k = \tau_w \frac{C_\mu^{1/4} k^{1/2}}{\kappa \eta} \tag{17}$$

where τ_w is the wall shear stress and η is the distance from the cell center of wall-adjacent cells to the wall. The above formulation of the turbulent production term introduced by Pope (2000) was based on the assumption of equilibrium state between turbulent production and turbulent dissipation rate. The other expression for the turbulent production term is

$$G_k = \tau_w \frac{\tau_w}{\rho \kappa \eta C_\mu^{1/4} k^{1/2}} \tag{18}$$

which was proposed by Launder and Spalding (1972). Hereinafter Eq.(18) is denoted by LS-WF while Pope-WF represents a near-wall treatment using Eq. (17). Table 5 compares resistance coefficients between LS-WF and Pope-WF. The difference of resistance coefficients between LS-WF and Pope-WF is less than 3% except for SST k-ω model at $\Delta\eta_{wall} = 0.012$ m. This means that the resistance coefficients are not as sensitive to the formulation of G_k as is $\Delta\eta_{wall}$.

In order to elucidate the sensitivity of ship resistance to near-wall treatment for friction velocity used in the boundary condition of effective viscosity in OpenFOAM, the formulation of η^* has to be discussed. When a wall function is utilized near the wall the friction velocity, u_τ, is explicitly assumed as follows:

$$-uv = u_\tau^2 = C_\mu^{1/2} k \tag{19}$$

where uv is Reynolds stress near the wall. The above expression of u_τ is derived from the balance of turbulent production and dissipation in simple turbulent shear flows,

$$\frac{|uv|}{k} = C_\mu^{1/2} \frac{G_k}{\varepsilon} \tag{20}$$

where ε is a turbulent dissipation rate. The expression of u_τ in Eq.(19) yields $\eta^* = \frac{C_\mu^{1/4} k^{1/2}}{\nu} \eta$, which can be explicitly used in the wall boundary condition of turbulent viscosity. Tables 3 and 4 show the resistance coefficients obtained when the friction velocity was calculated from Eq. (19), referred to hereinafter as EQ-FV. An alternative way of getting the friction velocity at the wall requires a little extra effort by iteratively adjusting u_τ until the log-law of Eq. (21) is satisfied when Eq. (11) gives the velocity (U) and distance (η) at the center of wall-adjacent cells, which we later refer to as LOG-FV.

$$\frac{U}{u_\tau} = \frac{1}{\kappa} \log\left(E \frac{\eta u_\tau}{\nu}\right) \tag{21}$$

However the application of LOG-FV is acceptable only if the wall-adjacent cells are located in the log region of turbulent boundary layers. To overcome the limitation of LOG-FV Spalding (1961) proposed a unified law of the wall that covers both the viscous and inertial sublayers as follows:

$$\eta^* = U^* + e^{-\kappa B}\left(e^{-\kappa U^*} - 1 - \kappa U^* - \frac{(\kappa U^*)^2}{2} - \frac{(\kappa U^*)^3}{6}\right) \tag{22}$$

where B is $\kappa^{-1} \log(E)$. Hereinafter SPALDING-FV represents a numerical procedure for the friction velocity to satisfy the unified law of Eq. (22) instead of the log-law in Eq. (21). Although SPALDING-FV is not free from the inherent limitation that the unified law is only

Table 5
Sensitivity of resistance coefficients to the production of turbulent kinetic energy.

G_k	$\Delta\eta_{wall}$ (m)	$\Delta\eta^+_{(avg)}$	Realizable k-ε model			SST k-ω model		
			C_{VM}	C_{PM}	C_{TM}	C_{VM}	C_{PM}	C_{TM}
LS-WF	0.0015	38	2.799	0.901	3.700	2.823	0.899	3.722
	0.0030	73	2.787	0.898	3.685	2.721	0.894	3.615
	0.0060	118	2.765	0.889	3.654	2.602	0.914	3.516
	0.0120	191	2.740	0.950	3.690	2.522	0.908	3.430
Pope-WF	0.0015	37	2.821	0.898	3.719	2.780	0.900	3.681
	0.0030	70	2.790	0.890	3.679	2.678	0.892	3.570
	0.0060	111	2.741	0.889	3.630	2.555	0.920	3.475
	0.0120	164	2.667	0.959	3.625	2.266	0.912	3.178

*The values of C_{VM}, C_{PM} and C_{TM} are scaled by 10^3.
**The wall unit of $\Delta\eta$ is calculated by using friction velocities of SST k-ω model.

valid for turbulent velocity profiles with zero gradient of pressure, one undeniable fact is that as long as a wall function is used for near-wall treatment Spalding's law of Eq. (22) is a more generalized form than the log-law.

A comparison of resistance coefficients among EQ-FV, LOG-FV and SPALDING-FV is made in Table 6. Note that when the friction velocity is calculated from the turbulent kinetic energy of EQ-FV C_{VM} and C_{TM} reduce by almost 11% and 8% in SST k-ω model as $\Delta\eta_{wall}$ increases. When u_τ is iteratively adjusted by LOG-FV the reduction of C_{VM} and C_{TM} are less than 5% and 4% in SST k-ω model. For SPALDING-FV C_{VM} and C_{TM} reduce by less than 4% and 3% as $\Delta\eta_{wall}$ increases. It is clear that the ship resistance of SST k-ω model is more robust against the change of $\Delta\eta_{wall}$ when either the log-law or Spalding's law is used to adjust the friction velocity than when u_τ is explicitly calculated from the turbulent kinetic energy. To check the validity of EQ-FV, LOG-FV and SPALDING-FV, the corresponding $\Delta\eta^+$ to each height was also calculated by using friction velocities of SST k-ω model. Because the Reynolds number corresponding to a 7 m-length model ship at 2 m/s speed is high, the $\Delta\eta^+$ is reasonably assumed to be in the log-region of turbulent boundary layer except for $\Delta\eta_{wall} = 0.0015$ m. The wall unit of $\Delta\eta^+ \approx 37-38$ is located on the border of buffer and log layers. In realizable k-ε model, even though the variation of C_{VM} does not reduce as much as that of SST k-ω model, the C_{VM} reduction (1% and 2%) for LOG-FV and SPALDING-FV is almost at the same level of 2% for EQ-FV as $\Delta\eta_{wall}$ increases. Note that the results of LOG-FV and SPALDING-FV are very similar except for $\Delta\eta_{wall} = 0.0015$ m. Because the essence of LOG-FV and SPALDING-FV based on empirical laws near the wall are the same and the log-law is more popular in practical engineering, we further elaborate distinct features of EQ-FV and LOG-FV.

Fig. 6 plots the x component of wall shear stress when the friction velocity is obtained from LOG-FV. A difference of wall shear stress between Fig. 4 for EQ-FV and Fig. 6 for LOG-FV is observed in the bulbous bow. The dependence of wall shear stress on $\Delta\eta_{wall}$ for EQ-FV means that the observation of low τ_w in the entrance of vessel is attributed to numerical characteristics of EQ-FV rather than physical phenomena observed in real experiments. Because turbulence stimulators installed in the bulbous bow give rise to enhancement of turbulent fluctuations in real experiments and the qualitative similarity of wall shear stress observed in the bulbous bows of Fig. 6 as $\Delta\eta_{wall}$ increases, the spatial distribution of wall shear stress obtained from LOG-FV is expected to be more reasonable. The friction velocity obtained from LOG-FV is compared with u_τ of EQ-FV in Fig. 7 when SST k-ω model is used at $\Delta\eta_{wall} = 0.012$ m. This shows that the calculation of friction velocity

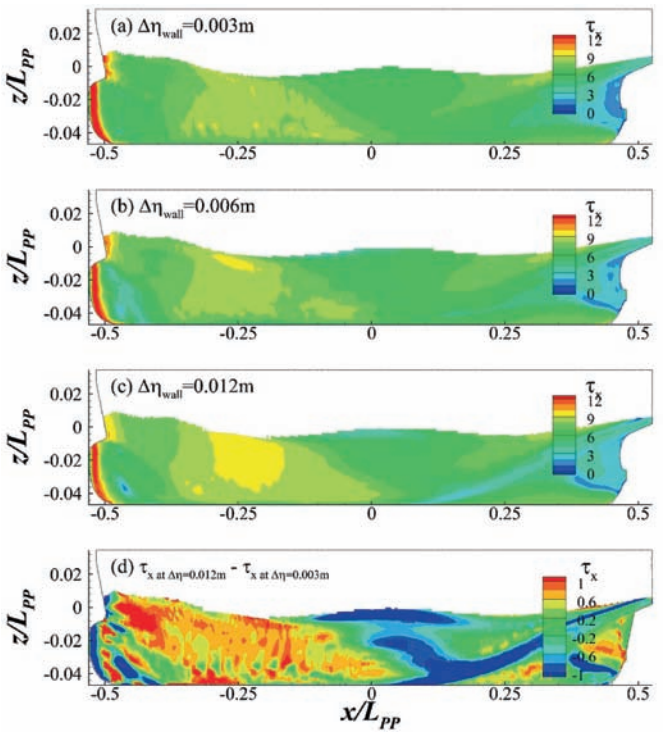

Fig. 6. Sensitivity of wall shear stress on hull to the height of wall-adjacent cells when the friction velocity is estimated from the log-law (LOG-FV).

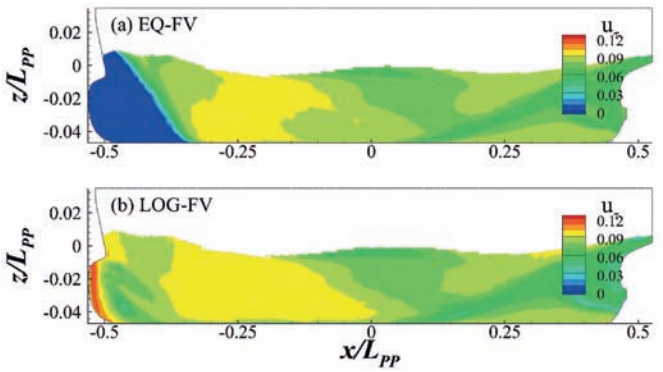

Fig. 7. Comparison of friction velocity between EQ-FV and LOG-FV when $\Delta\eta_{wall} = 0.012$ m.

Table 6
Sensitivity of resistance coefficients to calculation of friction velocity.

u_τ	$\Delta\eta_{wall}$ (m)	$\Delta\eta^+_{(avg)}$	Realizable k-ε model			SST k-ω model		
			C_{VM}	C_{PM}	C_{TM}	C_{VM}	C_{PM}	C_{TM}
EQ-FV	0.0015	38	2.799	0.901	3.700	2.823	0.899	3.722
	0.0030	73	2.787	0.898	3.685	2.721	0.894	3.615
	0.0060	118	2.765	0.889	3.654	2.602	0.914	3.516
	0.0120	191	2.740	0.950	3.690	2.522	0.908	3.430
LOG-FV	0.0015	37	2.772	0.899	3.671	2.776	0.911	3.687
	0.0030	73	2.766	0.895	3.661	2.714	0.895	3.610
	0.0060	128	2.756	0.890	3.646	2.671	0.906	3.576
	0.0120	218	2.752	0.943	3.695	2.659	0.909	3.568
SPALDING-FV	0.0015	37	2.805	0.899	3.704	2.759	0.912	3.671
	0.0030	74	2.799	0.891	3.691	2.727	0.893	3.620
	0.0060	129	2.771	0.889	3.660	2.687	0.908	3.595
	0.0120	219	2.758	0.942	3.700	2.666	0.905	3.571

*The values of C_{VM}, C_{PM} and C_{TM} are scaled by 10^3.
**The wall unit of $\Delta\eta$ is calculated by using friction velocities of SST k-ω model.

in near-wall treatment is mainly responsible for the distribution of wall shear stress on the bulbous bow.

In order to quantitatively compare the friction velocities calculated in LOG-FV and EQ-FV, the new coordinate of ξ corresponding to the water line of hull at $y = -0.15$ m is introduced as illustrated in Fig. 8(a). Comparisons of turbulent kinetic energy and its budget analysis on the wall adjacent-cells between EQ-FV and LOG-FV are made in Fig. 8(b) and (c). Based on the development of turbulent kinetic energy along the ξ-axis three zones can be characterized: a weak turbulence zone where little turbulent kinetic energy is produced, a non-equilibrium zone where the production of turbulent kinetic energy (G_k) is partially convective ($\nabla\cdot(\rho k\vec{U})$) and partially dissipated ($\beta^*\rho\omega k$) and an equilibrium zone where the production of turbulent kinetic energy is balanced with the turbulent dissipation. Among these zones the friction velocity of the weak turbulence zone is noticeable in Fig. 9 which shows the

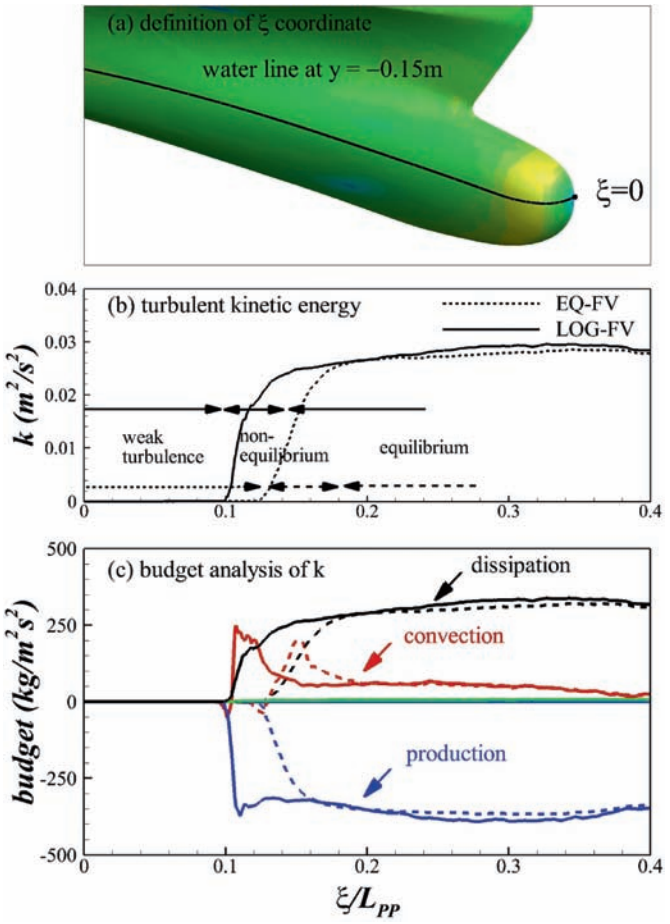

Fig. 8. Comparisons of turbulent kinetic energy and its budget analysis along a water line at $y = -0.15$ m between EQ-FV and LOG-FV when $\Delta\eta_{wall} = 0.012$ m.

velocity gradient normal to the wall and the friction velocity at the wall when EQ-FV is used. The friction velocities of $\Delta\eta_{wall} = 0.006$ m and 0.012 m along the ξ-axis are very different although similar distributions of the velocity gradient appear. This means that the observation of very small u_τ in the weak turbulence zone is a numerical feature of EQ-FV depending on $\Delta\eta_{wall}$. Since $u_\tau = C_\mu^{1/4} k^{1/2}$

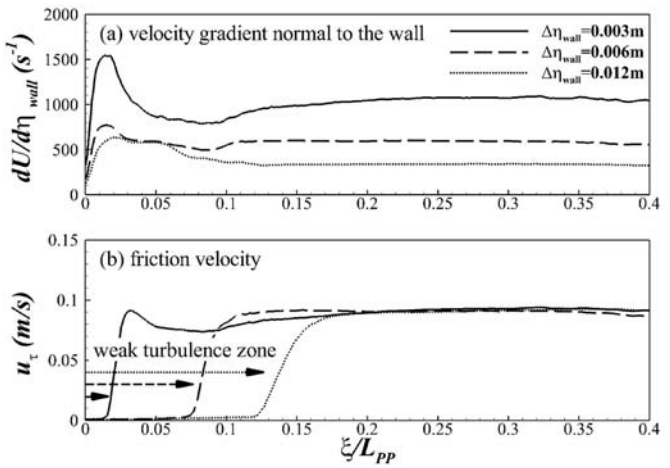

Fig. 9. Dependences of velocity gradient normal to the wall and friction velocity at the wall on $\Delta\eta_{wall}$ when EQ-FV is used.

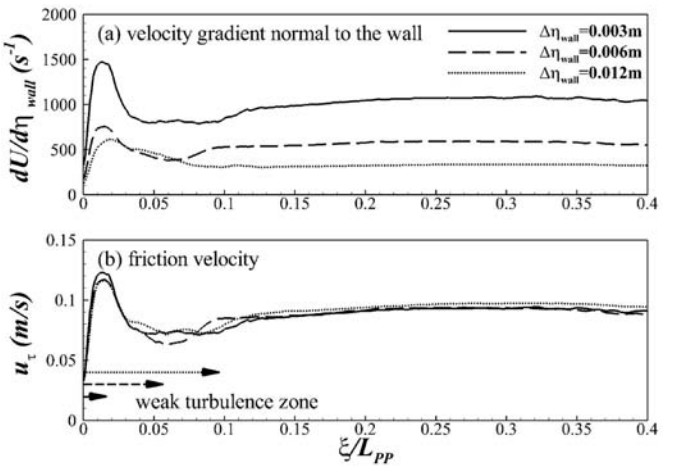

Fig. 10. Dependences of velocity gradient normal to the wall and friction velocity at the wall on $\Delta\eta_{wall}$ when LOG-FV is used.

is valid for an equilibrium state between the production and dissipation of turbulence the limitation of EQ-FV is definitely disclosed in the weak turbulence and non-equilibrium zones. In Fig. 10, however, the friction velocities of LOG-FV are very similar along the ξ-axis regardless of $\Delta\eta_{wall}$ even in the zones of weak turbulence and non-equilibrium. It is concluded that the independence of u_τ on the height of wall-adjacent cells makes LOG-FV more useful than EQ-FV. To check the predictability of resistance coefficients when LOG-FV and SPALDING-FV are used instead of EQ-FV, Fig. 11 shows the tendency of resistance coefficients as $\Delta\eta_{wall}$ increases. Similar to the results of EQ-FV that Fig. 2 showed,

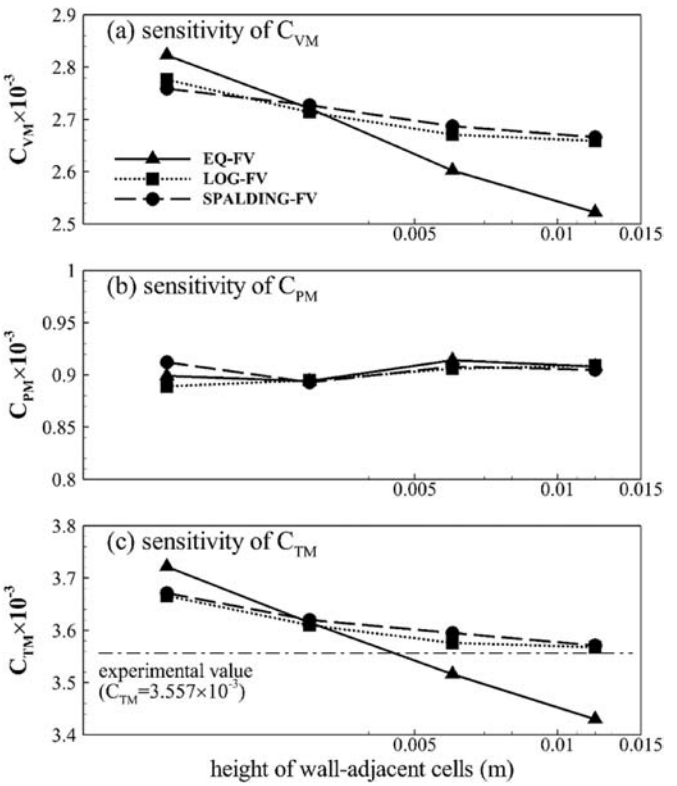

Fig. 11. Sensitivity of resistance coefficients to the height of wall-adjacent cells when the friction velocity is calculated from EQ-FV, LOG-FV and SPALDING-FV respectively.

Table 7
Sensitivity of resistance coefficients to the stretching ratio of prism layers.

Stretching ratio	Number of layers	Total thickness of layers (m)	SST k-ω model		
			C_{VM}	C_{PM}	C_{TM}
1.1	9	0.04074	2.723	0.879	3.602
1.3	6	0.03827	2.714	0.895	3.610
1.5	5	0.03956	2.709	0.906	3.615

*The values of C_{VM}, C_{PM} and C_{TM} are scaled by 10^3.

Table 8
Sensitivity of resistance coefficients to the thickness of prism layers.

Total thickness of layers (m)	Number of layers	SST k-ω model		
		C_{VM}	C_{PM}	C_{TM}
0.01197	3	2.707	0.931	3.638
0.03827	6	2.714	0.895	3.610
0.12786	10	2.725	0.885	3.609

*The values of C_{VM}, C_{PM} and C_{TM} are scaled by 10^3.

C_{VM} and C_{TM} of LOG-FV and SPALDING-FV are logarithmically proportional to the height of wall-adjacent cells while C_{PM} shows little change. This means that the ship resistances of KCS are very predictable at a given height of wall-adjacent cells.

Now sensitivity of ship resistance to stretching ratio (r) and total thickness (δ) of the prism layers near the hull will be studied because the prism layer is generated by a geometric progression with $\Delta\eta_{wall}$, r and δ. We use stretching ratios of 1.1, 1.3 and 1.5 to generate prism layers near the hull in unstructured grids while we fix the height of wall-adjacent cells at 0.003 m. The number of prism layers is chosen in order to keep the total thickness of prism layers constant at as near 0.04 m as possible. Table 7 lists the resistance coefficients of SST k-ω model when LOG-FV is used instead of EQ-FV. Because the variation of C_{VM} and C_{TM} is less than 1% as r grows the ship resistance is insensitive to the stretching ratio of prism layers. Next we set the total thickness of prism layers to 0.01197 m, 0.038268 m and 0.127858 m by controlling the number of layers while the constant height of wall-adjacent cells is 0.003 m. We apply the constant stretching ratio of 1.3 and use LOG-FV to calculate the friction velocity. The resistance coefficients of SST k-ω turbulence model are listed in Table 8. The change of total thickness of prism layers only slightly influences the resistance coefficients.

4. Conclusions

In the present study we performed numerical simulations of turbulent flows around KCS to study the sensitivity of ship resistance to wall-adjacent grids and disclose the influence of near-wall treatment on the sensitivity of ship resistance. Open source library, OpenFOAM, was utilized to predict ship resistance with a local time stepping scheme for temporal discretization while a linear interpolation with van Leer limiter was used as a flux limiter for physical properties. We compare the resistance coefficients of viscous and pressure forces when realizable k-ε and SST k-ω turbulence models were applied to structured and unstructured grids. The height of wall-adjacent cells was found to play the most important role in the prediction of ship resistance among other grid parameters while the stretching ratio and total thickness of prism layers had slight influence on the ship resistance. While the application of SST k-ω model to unstructured grids was attractive for prediction of the ship resistances as the height of wall-adjacent cells increased, we found the distribution of friction velocity responsible for the reduction of viscous and total resistances to be numerically affected by the height of wall-adjacent cells in the bulbous bow when the friction velocity was estimated from an assumption of equilibrium state between turbulent production and dissipation. Since the equilibrium assumption was not met in the bulbous bow, it was more reasonable to iteratively calculate the friction velocity from empirical laws of the wall rather than explicitly estimate it from the turbulent kinetic energy. By comparing the ship resistance when the friction velocity was calculated from the log-law and Spalding's law, we confirmed that the calculated resistance was very predictable at a specific height of wall-adjacent cells.

Acknowledgement

This research was supported by Basic Science Research Program through the National Research Foundation of Korea(NRF) funded by the Ministry of Science, ICT & Future Planning(NRF-2016R1C1B1010002)

References

Banks, J., Turnock, S.R., Hudson, D.A., Blake, J.I.R., Philips, A.B., 2010. RANS simulations of the multiphase flow around the KCS hull form. In: Gothenburg 2010; CFD Workshop in Ship Hydrodynamics, December 08–10, Gothenburg, Sweden.
Choi, J.-E., Min, K.-S., Kim, J.H., Lee, S.B., Seo, H.W., 2010. Resistance and propulsion characteristics of various commercial ships based on CFD results. Ocean Eng. 37 (7), 549–566.
Cowles, G.W., 2001. A Parallel Viscous Multiblock Flow Solver for Free Surface Flows Pas Complex Geometries. PhD thesis. Princeton University, Department of Mechanical and Aerospace Engineering.
Craft, T.J., Gerasimov, A.V., Iacovides, H., Launder, B.E., 2002. Progress in the generalization of wall function treatments. Int. J. Heat Fluid Flow 23 (2), 148–160.
Guo, B.J., Deng, G.B., Steen, S., 2013. Verification and validation of numerical calculation of ship resistance and flow field of a large tanker. Ships Offshore Struct. 8 (1), 3–14.
Kim, G.-H., Park, S., 2017. Development of a numerical simulation tool for efficient and robust prediction of ship resistance. Int. J. Naval Architec. Ocean Eng. 9 (5), 537–551.
Kim, W.J., Van, S.H., Kim, D.H., 2001. Measurement of flows around modern commercial ship models. Exp. Fluid 31 (5), 567–578.
Launder, B.E., Spalding, D.B., 1972. Lectures in Mathematical Models of Turbulence. Academic Press, UK.
Lee, S.B., 2014. Application of OpenFOAM to prediction of hull resistance. In: 9th International OpenFOAM Workshop, June 23–26, Zagreb, Croatia.
Menter, F.R., Kuntz, M., Langtry, R., 2003. Ten Years of Industrial Experience with the SST Turbulence Model. Turbulence, Heat and Mass Transfer, Begell House, Inc.
Park, S., Park, S.W., Rhee, S.H., Lee, S.B., Choi, J.-E., Kang, S.H., 2013. Investigation on the wall function implementation for the prediction of ship resistance. Int. J. Naval Architec. Ocean Eng. 5, 33–46.
Pope, S.B., 2000. Turbulent Flows. Cambridge University Press, UK.
Rusche, H., 2002. Computational Fluid Dynamics of Dispersed Two-phase Flows at High Phase Fraction. PhD thesis. Imperial College, London.
Spalding, D.B., 1961. A single formula for the law of the wall. Trans. ASME Series E: J. Appl. Mech. 28, 455–458.
van Leer, B., 1979. Towards the ultimate conservation difference scheme. J. Comput. Phys. 32 (1), 101–136.
Wilson, R.V., Stern, F., Coleman, H.W., Paterson, E.G., 2001. Comprehensive approach to verification and validation of CFD simulations – Part 2: application for RANS simulation of a cargo container ship. ASME J. Fluids Eng. 123, 803–810.